Journal of Power Sources 285 (2015) 1–11

Contents lists available at ScienceDirect

Journal of Power Sources

journal homepage: www.elsevier.com/locate/jpowsour

Effect of the porous structure of the support on hydrocarbon distribution in the Fischer–Tropsch reaction

Monica Bartolini [a, *], Jhoanna Molina [a], Juan Alvarez [a], Mireya Goldwasser [a], Pedro Pereira Almao [b], M.Josefina Pérez Zurita [a, b]

[a] Universidad Central de Venezuela, Facultad de Ciencias, Escuela de Química, Centro de Catálisis, Petróleo y Petroquímica, Caracas, Venezuela
[b] University of Calgary, Schulich School of Engineering, Calgary, Canada

HIGHLIGHTS

- We synthesize and evaluate catalysts to produce diesel fraction components in FTS.
- Pore diameter significantly influences the liquid products distribution.
- The catalyst with smaller pore size showed a deviation from the ASF mechanism.

GRAPHICAL ABSTRACT

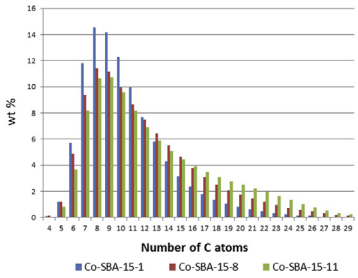

ARTICLE INFO

Article history:
Received 28 October 2014
Received in revised form
13 February 2015
Accepted 12 March 2015
Available online 14 March 2015

Keywords:
Fisher–Tropsch
SBA-15
Cobalt
Shape selectivity

ABSTRACT

Emissions standards are increasingly stringent due mainly to its impact on the environment. Although the diesel engine is an attractive solution for carbon dioxide reduction, a challenge remains to simultaneously control nitrogen oxides and matter particulate emissions to accepted levels. On engine tests, it has been observed that Fischer–Tropsch diesel significantly reduces CO, HC, PAHs and particulate emissions compared to oil derived diesel. However, selectivity control in Fischer Tropsch Synthesis is still a key challenge due the Anderson-Schultz-Flory polymerization mechanism followed by hydrocarbon distribution. In this work we are presenting the first steps towards a new strategy that can tune, in one step, the selectivity to desired products by taking advantage of the shape selectivity properties of SBA-15 mesoporous silica used as support.

Co-SBA-15 (30%wt) catalysts with different pore size were prepared by excess solution impregnation. Our results show that pore diameter not only affects the size and reducibility of Co particles but it also significantly influence the liquid products distribution, with the high molecular weight hydrocarbon fraction increasing on large pores, attributed to the existence of a shape selectivity effect induced by the textural properties of the catalyst namely its pore size and pore volume.

1. Introduction

The production of clean fuels, particularly diesel, by means of Fischer–Tropsch synthesis (FTS) has sparked renewed interest in recent years both in industry and academia. The predominantly linear paraffinic hydrocarbons produced in the FTS, along with virtually no contaminants such as sulfur, nitrogen and aromatics, produce FT diesel with higher cetane number (≥75) [1] and lower pollutant emission levels than a refinery diesel. Due to the typical

* Corresponding author.
E-mail address: danmon15@hotmail.com (M. Bartolini).

http://dx.doi.org/10.1016/j.jpowsour.2015.03.081
0378-7753/

Anderson-Schultz-Flory (ASF) polymerization mechanism [2], it is possible to obtain in a single step, high selectivity to hydrocarbons with a very narrow boiling point range. Because of this, FT processes aiming to produce synthetic diesel, uses catalysts that have a high selectivity to high molecular weight (waxes) linear alkanes which, subjected to a subsequent mild hydrocracking process, maximize diesel production, while their properties are further improved by isomerization of the linear alkanes.

Several excellent reviews have been published on the Fischer Tropsch Synthesis and some concepts have been established [3–6]. Most existing catalysts designed to obtain a high selectivity to waxes in the FTS use cobalt as main active metal supported on a porous inorganic oxide (SiO_2, Al_2O_3, TiO_2), together with one or more promoters. The activity of these catalysts is proportional to the concentration of Co surface, which depends essentially on two parameters: the reduction degree (RD) of cobalt oxide reached during the catalyst reduction step prior to the FTS and the dispersion of the reduced cobalt. These two parameters are generally related to each other and are largely determined by the Co-support interaction. Thus, when TiO_2 is used as support, the strong interaction between Co and TiO_2, favors a high metal dispersion but results in the formation of low reducibility of Co species, giving rise to a low concentration of active sites. In contrast, the weak interaction between Co–SiO_2 favors Co particles reduction. However, they tend to agglomerate leading to relatively low dispersions. The behavior of Co supported on Al_2O_3 is generally intermediate between that shown by Co on TiO_2 and SiO_2. It has also been established that the efficiency of this reaction can be greatly improved by designing new thermally stable catalysts with good mechanical and heat transfer properties, minimizing hot spots developed in the catalyst bed, which promote metal particle sintering.

In the last decade, several authors have explored the possibility of employing mesoporous silicas as an alternative for Co based F-T conventional supports [7–16]. In particular the high surface area ordered mesoporous materials (>800 m^2 g^{-1}) and its regular porous structure, with narrow pore diameter distribution, allows for a higher Co dispersion even at high metal loadings and can exerts control on the metal particle size distribution, which influence their catalytic properties.

However, the effect of the porous structure of the support on hydrocarbon distribution in the FT reaction remains not well understood and is still subject of controversy. All these studies have suggested that the pore size distribution could significantly affect the Fischer–Tropsch Synthesis reaction rate and hydrocarbon selectivity but the way it occurs remains unclear. Okabe et al. [7] reported that wide pore catalysts are preferable for higher conversion and higher C5+ selectivity because of the higher reducibility of large cobalt particles in wide pores over the pore size range from 4 to 10 nm. In an early study, Anderson et al. [8] reported that the FTS activity and selectivity of cobalt based catalyst could be affected by their pore sizes. The observed increase in methane selectivity with decreasing average pore size was attributed to mass transport phenomenon. However, Lapszewicz et al. [9] years later reported that the variation of product distribution as a function of catalyst pore diameter was a result of the change of adsorption patterns of hydrogen and carbon monoxide rather than mass transfer phenomena. The analysis of Lapszewicz data seems to suggest that this change of adsorption patterns is related to the particle size which in turn relates very well with pore diameter. Ernst et al. [10] studied the FT activity and selectivity of Co/SiO_2 prepared by a sol–gel technique in acid and base media. It was found that the activity for FT increased with the specific surface area, and the selectivity for higher molecular weight hydrocarbon was favored when the pore diameter was lower than 4 nm. Khodakov et al. [11] investigated the pore size effects on Fischer–Tropsch reaction rates and selectivities over cobalt catalysts using periodic (SBA-15 and MCM-41) and commercial mesoporous silicas as supports. They found that the Fischer–Tropsch reaction rates and C5+ selectivity were much higher on cobalt catalysts with the support pore diameter exceeding 3 nm than on the narrower pore catalysts. Iglesia et al. [12] reported that hydrocarbon product selectivity depends on a complex interplay between diffusion, reaction and convection processes occurring within the catalyst pellets and reactors. A structural parameter χ, which includes parameters such as pellet radius, pellet porosity, mean pore radius of support and active metal distribution on support, seems to play a vital role in determining the Fischer–Tropsch activity and selectivity. Feller et al. [13] and Saib et al. [14] showed evidence of the role of pore diameter on cobalt cluster size stressing on the fact that with increasing cluster size, a strong increase in the extent of secondary reactions occurs i.e. olefin readsorption. According to Saib et al. [14], activity of the supported cobalt catalysts in the Fischer–Tropsch synthesis seems to be a function of the metal dispersion and the extent of deactivation during the Fischer–Tropsch synthesis while the C5+-selectivity could be described using the reactant transport model proposed by Iglesia et al. [12] and is a function of conversion. Xiong et al. [15] studying the role of pore size in Co/SBA-15 catalysts also concluded that catalysts with larger pores led to larger cobalt cluster size, lower dispersion and higher reducibility and gave rise to more bridge type CO adsorbed on FTS. They also stated that catalysts with larger cobalt cluster size showed higher C5+ selectivity in the FTS. The reported results are very solid and clear evidences have been shown in all cases supporting the author claims. However, we believe that an additional factor i.e. shape selectivity also plays a role.

We previously reported [16] on the possibility of a shape selectivity effect of mesoporous structures (namely HMS) on the shaping of the liquid product distribution in the FTS reaction. The present work deals with the study of the behavior of cobalt on SBA-15 mesoporous silica, which will support our previous findings since its pore size could easily be changed by means of using a swelling agent and controlling synthesis conditions.

A mixture of a triblock copolymer: polyethylene oxide/polypropylene oxide/polyethylene oxide (EO/PO/EO), was used as surfactant in SBA-15 molecular sieve synthesis with different pore size, possessing two kinds of moieties, i.e. the hydrophilic EO block and the hydrophobic PO block. The micellization of the triblock copolymers are driven by the hydrophobic polyethylene oxide (PO) block with a core consisting of PO blocks and a corona of EO blocks [7]. SBA-15 pore size is mainly determined by the hydrophobic part of the micelles and can be changed by controlling synthesis conditions.

2. Experimental

2.1. Supports synthesis and characterization

SBA-15 mesoporous silica with different pore sizes were synthesized using Pluronic P123 ($EO_{20}PO_{70}EO_{20}$, M_{AV} = 5800, BASF) and tetraethyl orthosilicate (TEOS) under acidic conditions, following the methodology proposed by Wang et al. [17]. 10 g of P123 were added to 350 mL of 2 M HCl solution at 35 °C to obtain a clear solution. Then 21 g of TEOS were added drop wise under vigorously stirring for 48 h. The obtained white solid was recovered by vacuum filtration, washed several times with distilled water and air-dried overnight at 80 °C. Organic molecules occluded in the mesopores were removed by direct calcination at 500 °C with air flow for 6 h. The small pore size silica support (SBA-15-1) was synthesized without any hydrothermal treatment. In order to

obtain supports with higher pore diameters two additional steps were taken: the addition of a co-surfactant and a post synthesis heat treatment (PSHT) as reported by Katiyar et al. [18] and Phuong et al. [19]. Trimethylbenzene (TMB) was used as co-surfactant and added to the homogeneous mixture using a 0.26 and 1.0 TMB/P123 ratio followed by a post-synthesis heat treatment at 120 °C during 24 h to produce supports SBA-15-8 and SBA-15-11 respectively.

Nitrogen isotherms at −196.15 °C were measured by means of a Micromeritics TriStar 3000 apparatus. Prior to the adsorption measurements, the samples were out gassed overnight at 250 °C. Nitrogen isotherms were obtained in both adsorption and desorption modes. The surface areas of supports and catalysts were determined by the BET method and the total pore volume was calculated from the amount of N_2 adsorbed at a relative pressure (P/Po) close to unity, where P and Po are the equilibrium pressure over the solid and saturated vapor pressures of the gas at the liquid nitrogen temperature, respectively. Pore size distribution was established from the adsorption branches of the isotherms using the Barrett–Joyner–Halenda (BJH) method.

X-ray Diffraction (XRD) patterns were obtained for all the supports to determinate the ordering of the porous material, on RIGAKU, model ULTIMA III using a Cu source diffractometer. XRD patters were recorded at low angles (2θ sweep = 0.5° with a pitch of 0.2, 2 s/step).

2.2. Catalysts synthesis and characterization

The three synthetized supports with a small (50 Å), medium (107 Å) and large (146 Å) pore size were used in the preparation of the catalysts. Cobalt incorporation (30% w/w in all cases) was carried out by excess solution impregnation, using a hexahydrated cobalt (II) nitrate salt. The excess solution was evaporated at 60 °C in a rotor evaporator.

Catalysts composition was determined by Inductively Coupled Plasma (ICP) technique, using IRIS Intrepid II XDL equipment. Textural Properties of the catalysts were determined similarly as for the supports. For the XRD analysis, the same apparatus was used as for the supports to identify the phases and to calculate the average particle size of the crystallites by means of the Scherrer's equation ($d = (K^*\lambda^*180°)/(B^*\cos\theta^*\pi)$) [20,21]. The sweeping used for all the samples was from 5° to 70° at a rate of 2° min^{-1}. JCPDS-ICDD standard spectra software was used to determine the crystallographic phases.

TPR profiles were obtained to determine the reducibility of Co species in the calcined catalyst, using a ThermoQuest 1100 equipment from CE Instrument. A sample of around 100 mg was placed in a quartz tubular reactor and heated from room temperature to 1000 °C or 400 °C using a mixture of 10% H_2 balanced with Ar at a flow rate of 15 mL min^{-1} with a heating rate of 10 °C min^{-1}.

TEM analysis was used to determine the order, morphology and the crystallite particle size of the studied samples. Approximately 0.2 g of material were mixed with 2 mL of absolute ethanol, and a drop of the solution was deposited on a Cu grid. The analysis was performed in an H-7650 Hitachi 60 kV microscope.

XPS spectra was recorded in a VersaProbe PHI-5000 XPS, using monochromatic Al source (1486.6 eV) 49.3 W with a beam diameter of 200.0 microns. All spectra were calibrated with the binding energy of carbon 1s electrons (284.8 eV).

2.3. Catalytic tests

Activity tests were performed in a down-flow fixed-bed stainless-steel reactor (I.D. = 10 mm, l = 30 cm), loaded with 300 mg of catalyst. Prior to the catalytic tests the catalysts were reduced in situ at atmospheric pressure with hydrogen at 400 °C for 12 h using a heating rate of 2 °C/min. For all the catalysts, after the reduction step, the temperature was lowered to 190 °C under a hydrogen atmosphere and the reactant gas mixture (H_2:CO:N_2, 63:32:5, v/v, N_2 as internal standard) was fed at a total flow rate of 35 mL min^{-1} (GHSV = 7000 mL (NTP)/(gcat h), slowly increasing the system pressure up to 300 psi. The temperature in the catalytic bed was increased afterward from 190 °C to 230 °C at 2 °C min^{-1}. Once the reaction temperature was achieved, the reaction was led to proceed for 120 h. During reaction, the reactor effluent passed through a hot trap kept at 150 °C and 300 psi to collect waxes, and products leaving this trap were passed through a second trap kept at 3 °C and 300 psi to collect the lighter products (water, alcohols and hydrocarbons). The effluent gases were depressurized and analyzed periodically by on-line gas chromatography. Analyses were performed in various chromatographs according to the sample analyzed. Permanent gases and light hydrocarbons were analyzed on-line in a Perkin Elmer 3000 GC Auto system fitted with TCD and FID detectors using a Carbosieve SII Supelco column and an Alumina RT column, respectively. Liquid products (collected at 150 °C and 3 °C) were weighted and analyzed using two chromatographs. The liquid hydrocarbons were analyzed in a Varian 3300 fitted with a 30 m long Supelco Alumina KCl capillary column connected to a FID. The aqueous products were analyzed in a Varian series 3300 with a Porapack Q column connected to TCD.

3. Results and discussion

3.1. Support characterization

Table 1 shows the textural properties of synthesized SBA-15 mesoporous silica. It is observed that surface areas are similar to those reported for this type of materials [17]. Both, the PSHT and the addition of a co-surfactant had the expected effect: an increase in the pore diameter and pore volume with little effect on surface area.

All isotherms are type IV exhibiting the hysteresis condensation and evaporation steps characteristic of periodic mesoporous materials. Fig. 1 shows an example of isotherm obtained for the support SBA-15-1.

The effect of the addition of a co-surfactant on the textural properties of the materials is shown in Table 1. Evidently, the presence of TMB causes an increase in the pore size due to its incorporation readily into the *micelle*, increasing its width and consequently the volume and pore diameter of the resulting solid [18,19]. The pore size expansion can be explained on the basis that TMB being a no polar compound dissolves inside the triblock copolymer assemblies, thus increasing the volume of the hydrophobic moiety, so the pore size increases. Furthermore, higher temperature and longer reaction time result in larger pore sizes and thinner pore walls due to PEO hydrophilicity temperature dependence, which increases as temperature increases, as reported by Dalai and Davis [8]. Besides, at low temperature, the segments of the triblock copolymer are in an amorphous state and they tend to stretch as temperature increases. Similarly, not only the segment of

Table 1
Textural properties of synthesized supports.

Solids	Post-synthesis heat treatment (temperature, time)	TMB/P123	S_{BET} ($m^2\ g^{-1}$)	Pore diameter (adsorption) (nm) (BJH)	Pore volume ($cm^3\ g^{-1}$)
SBA-15-1	–	0	813	5	0.77
SBA-15-8	(120 °C, 24 h)	0.26	815	11	1.50
SBA-15-11	(120 °C, 24 h)	1	716	15	2.00

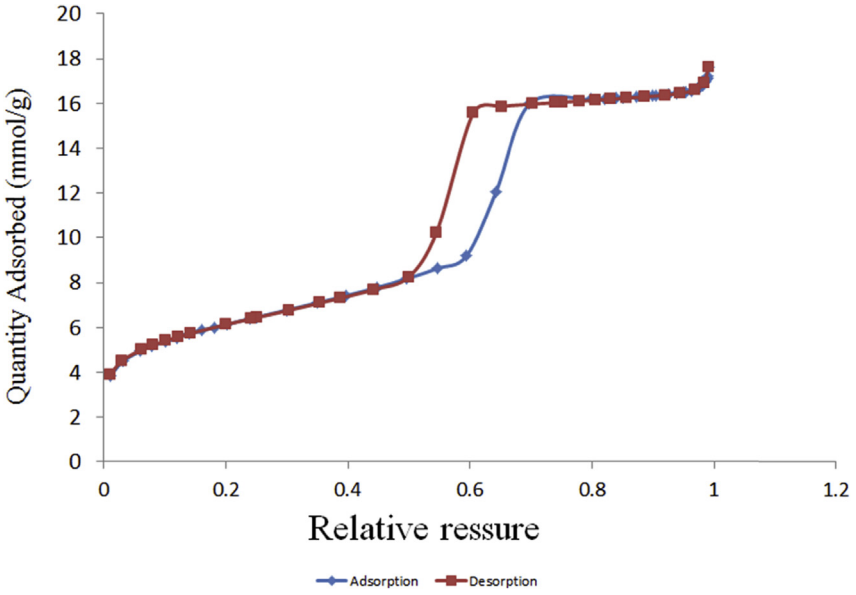

Fig. 1. Isotherms of SBA-15-1.

the PPO is longer than that of the PEO but also the hydrophobic segment of the PEO becomes longer at higher temperature, hence the hydrophobic volume increases and the pore wall tends to be thinner. Our results indicate that an efficient combination of PSHT and TMB promotes growth of both, the pore size and the pore volume.

A small decrease in the specific surface area was observed when TMB, was added to the synthesis medium. As will be seen on the XRD results, the solid array was significantly reduced when TMB content increases; indicating that a less organized structure can lead to a decrease in the specific surface area.

Fig. 2 shows the diffraction patterns of the three SBA-15 supports synthesized in a conventional way (SBA-15-1) and after adding the co-surfactant followed by the PSHT (SBA-15-8 and SBA-15-11). The SBA-15-1 support showed an intense peak at low angles ($2\theta \approx 1$), and secondary signals of lower intensity at slightly higher angles ($1.4^\circ < 2\theta < 2.2^\circ$) as shown in the insert. The intensity and good resolution of these peaks are associated with highly ordered structures. For the SBA-15-8 and SBA-15-11 supports a shift to lower 2θ angles occurs, which difficult observation of the most intense peaks. This shift is associated to the presence of larger pore diameters on these solids. The comparison of the degree of structural ordering of these solids was mainly based on secondary peaks analyses shown in the insert. For both supports SBA-15-8 and SBA-15-11, secondary peaks were very weak evidencing a poor structural order. When TMB is added to the synthesis solution with a fixed amount of surfactant, it would lead to the largest degree of swelling because TMB would be incorporated into the core of the hydrophobic micelles causing a deformation in the arrangement of the molecules that conform the micelles. The addition of even a small amount of TMB is believed to significantly disturb or even breaks up the micelles of the copolymer surfactant, resulting in a significant loss of the structural ordering of SBA-15 typical hexagonal structure.

3.2. Catalysts characterization

Table 2 shows the chemical composition and textural properties of the studied catalysts. A close similarity between the analytical and nominal values of the cobalt content was observed. As mentioned above, the specific surface area, pore volume and pore diameter obtained for the SBA-15 supports are in the order of magnitude reported for mesoporous systems. However, the addition of cobalt produces a decrease in the specific surface areas with Co-SBA-15-1 showing the larger reduction compared to the respective support. A dilution effect could be invoked in all cases, however, it does not account for the totality of the reduction observed because a dilution effect would produce a 30% reduction while the actual reduction is more than 50%. Due to the fact that Co-SBA-15-1 has the smaller pore diameter plugging of the pores during impregnation could account for the higher loss observed. In the other two catalysts, a third factor -partial collapse of the structure during impregnation/calcination-could be playing a role. A decrease in pore volume after metal impregnation on the support was observed for the three catalysts, indicating that part of the cobalt was located at the entrance and/or inside the pores. Regarding the pore diameter, no significant differences were observed between SBA -15-1 and the catalyst obtained impregnating this support (Co-SBA15-1). However, the pore diameter decreases for solids with intermediate and large pore sizes (Co-SBA15-8, Co-SBA15-11), suggesting that in these two catalysts, part of the Co is partially obstructing the pore mouth, reducing its size.

Fig. 3 shows the diffractograms of the studied catalysts. The characteristic signals at 36.8°, 65.4°, 59.4°, 44.8° and 31.3° 2θ angle reported for Co_3O_4 were observed (PDFWIN database N ° 42–1467).

Particle diameters calculated from the Scherrer equation using $2\theta = 36.8^\circ$ signal are reported in Table 2. The smaller pore size catalyst also show the smaller particle size, in agreement with what has been previously established that a small pore size limits the amount of impregnating solution (droplet size), giving rise to smaller and well distributed Co particles on the support surface [22–24]. Although an important difference in the pore size for catalysts Co-SBA-15-8 and Co-SBA-15-11 was observed no significant differences in particle size were observed by this method. This behavior could be attributed to the fact that, as mentioned above (Fig. 2) these supports have a less orderly structure which may lead to a wider particle size distribution.

TEM micrographs of Co-SBA-15-1, Co-SBA-15-8 and Co-SBA-15-11 catalysts are shown in Fig. 4 a–c. The parallel channels of the mesoporous support in Co-SBA-15-1 can clearly be seen in the

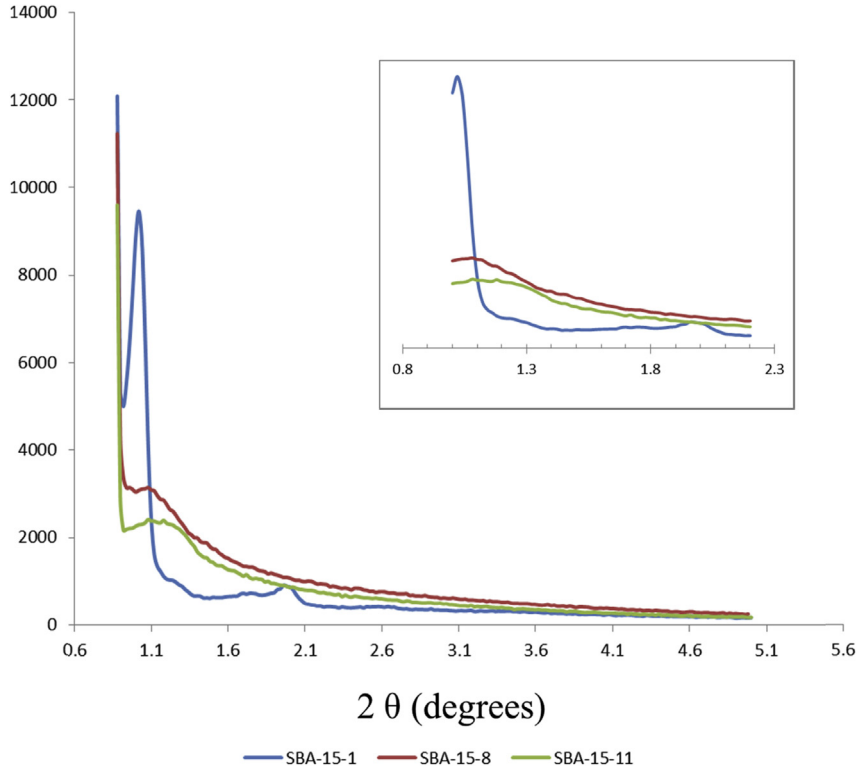

Fig. 2. XRD patterns of SBA-15 supports.

micrograph (Fig. 4a), indicating that the ordered structure of SBA -15-1 was maintained even after impregnation and calcination. On the contrary, a disorderly channel arrangement was observed for Co-SBA-15-8 and Co-SBA-15-11 (Fig. 4b and c) in agreement with XRD results, where a significant reduction of the intensity of the diffraction signals was observed. As previously discussed, an increase in TMB dosage, during the synthesis of the supports, evidently caused a phase transformation from ordered hexagonal to a mixture of disordered hexagonal and foam-like structure. In all cases, particles of cobalt oxide located inside the pores were evidenced along the longitudinal axis of the channels (Fig. 4a) and in the mouth of the pores (Fig. 4b and c). The presence of dark marks with larger diameters than the width of the channels, are attributed to cobalt oxide particles located outside the pores.

Fig. 5 shows the cobalt particle size distribution for the three catalysts. As expected, the pore diameter of the support has a strong effect on the obtained cobalt crystallite size for the preparation of mesoporous silica supported cobalt catalysts using cobalt nitrate: the obtained cobalt crystallite size increases with increasing pore diameter. It is also observed that the distribution of cobalt crystallites over the support is inhomogeneous. When increasing the support pore size, the crystallite size distribution becomes wider, indicating the important role play by the support on the metal particle size distribution. In the case of larger channels, where the amount of cobalt is higher, cobalt particles could agglomerate to form larger particles, favoring wider particle size distribution. Textural properties measurements support this observation. As seen in Table 2, catalysts with medium and large pore size showed a more significant reduction in the pore diameter for catalyst with a small pore size as compared with the respective supports. This suggests that cobalt accumulation in the pore mouth occurs in a bigger proportion for the catalyst with larger pore sizes, where the amount of cobalt per channel is higher. It is important to mention that, during the evaporation process of the impregnating solution, cobalt particles may move along the channel of the support favoring sintering.

Crystallite sizes obtained from TEM are shown in Table 3. The TEM crystallite sizes significantly differ from those obtained from the XRD analysis, differences becoming less important as the pore size increases. This result could be explained based on the intrinsic detection limitations of XRD for small particle sizes. Both, XRD and TEM results indicate that the small pores support has a high structural arrangement. Since all channels have the same dimensions, during the impregnation process, the amount of solution housed inside each channel should be approximately the same, favoring a narrow particle sizes distribution. XRD and TEM results showed a higher structural disorder for Co-SBA-15-8 and Co-SBA-15-11 catalysts, due to differences in the channel's size which, no being parallel to each other, intersect randomly and lead to the formation of cavities which allows accommodation of the impregnating solution and generates a wider particle size distribution.

Table 2
Catalysts chemical composition, textural properties and average particle size.

Solids	%Co (w/w) nominal	%Co (±1) w/w analytical	S_{BET} (m^2 g^{-1})	Dp (nm)	Pore volume (cm^3 g^{-1})	Particle size (nm) by XRD (±0.6)
Co-SBA-15-1	30	29	285	5	0.32	12.4
Co-SBA-15-8	30	31	357	7	0.66	18.7
Co-SBA-15-11	30	32	319	11	0.74	18.2

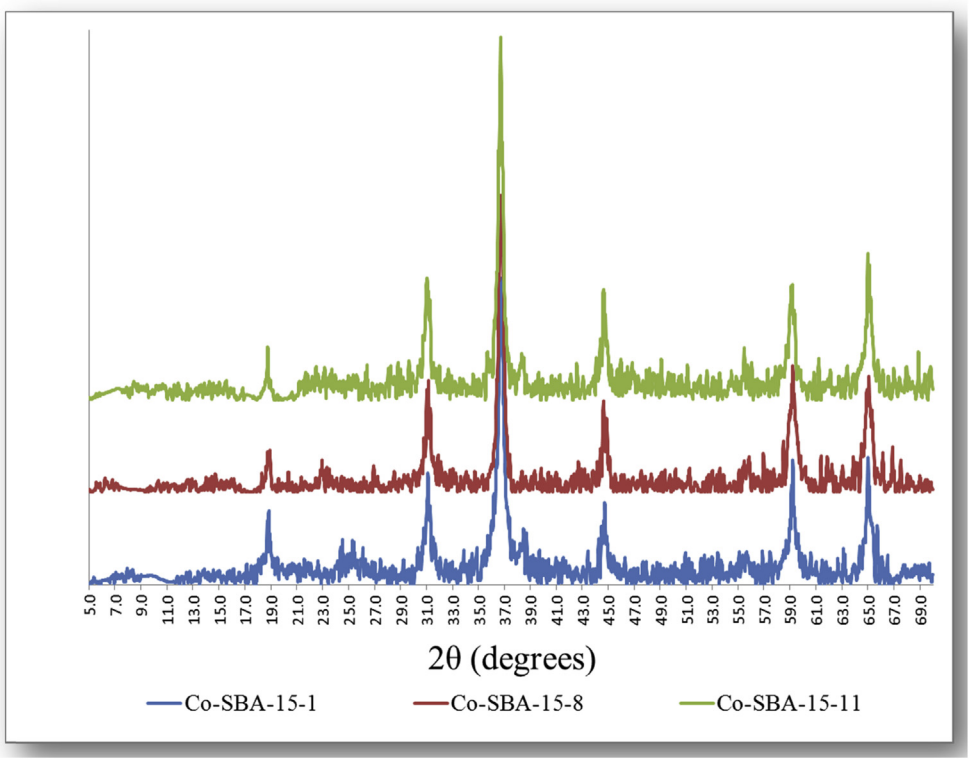

Fig. 3. XRD patterns of Co-SBA-15catalysts.

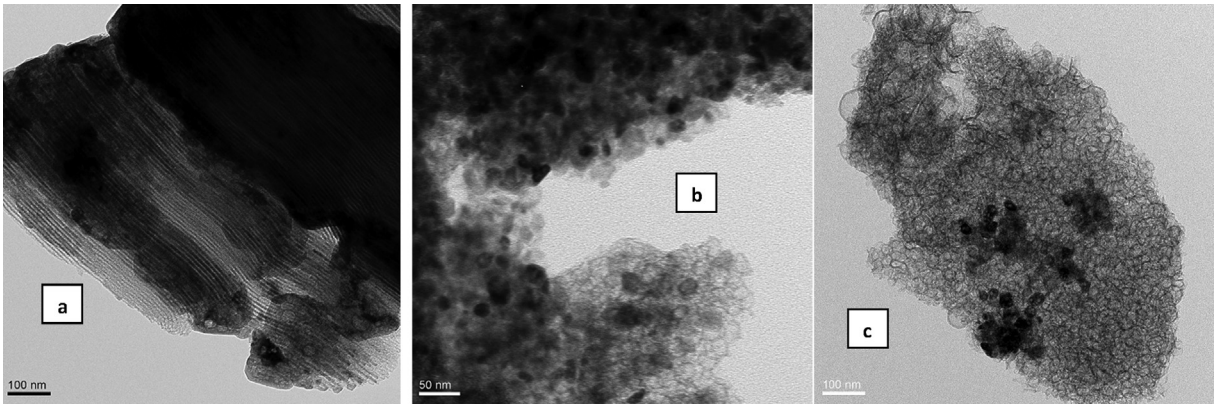

Fig. 4. TEM micrograph of (a) Co-SBA-15-1, (b) Co-SBA-15-8 and (c) Co-SBA-15-11 catalysts.

TPR profiles of synthesized catalysts are shown in Fig. 6. Three main bands were observed for all catalysts. The first reduction band may be associated with reduction of Co_3O_4 to CoO. The second reduction band is attributed to reduction of CoO to Co° [25]. As seen from Fig. 6, the second reduction step of Co-SBA-15-11 profile is wider and appears to be formed by the contribution of two bands. This result suggests that there are two different CoO species which reduce at two different temperatures. This interpretation is in agreement with TEM results that indicate a wider particle size distribution on this solid. As previously reported by Song et al. [22], the reducibility of supported species is highly influenced by the particle size of supported species. Smaller particles interacting strongly with the support are more difficult to reduce (higher Tmax), while larger particles can be more easily reduced.

The third reduction peak is broad and appears at temperatures above 600 °C, associated to species more difficult to reduce strongly interacting with the support, such as cobalt silicates. However, no direct evidence i.e. XRD signals were observed to assess the presence of this phase, possibly because particle size dimensions. Increasing the pore diameter of the catalyst decreases the size of the third peak Fig. 6. This result is in agreement with reported results [22–26] regarding the role of the support on the reducibility of the species. Larger pores lead to the formation of cobalt clusters easily reducible in contrast to small pores which favor the formation of smaller particles strongly interacting with the support and therefore more difficult to reduce. To study the reducibility of the catalyst under the conditions prior to catalytic tests, TPR experiments were conducted at 400 °C. After reaching the desired temperature, it was kept constant until H_2 consumption signal went back to zero (indicating that total reduction of the solid at that temperature occurred). Results are shown in Fig. 7. It can be observed that the first reduction peak coincides for the three

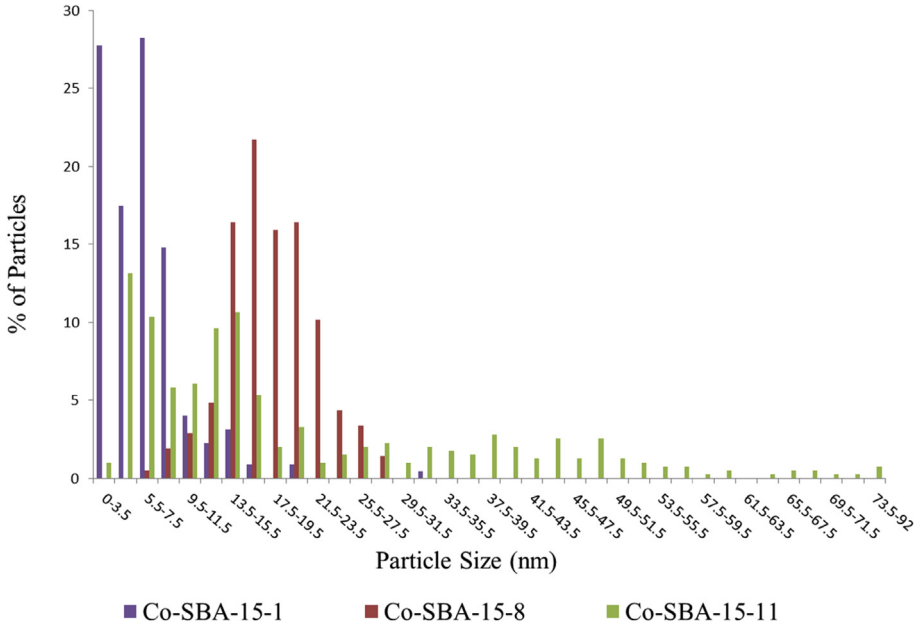

Fig. 5. Particle Size Distribution of Co-SBA-15 catalysts obtained from TEM analyses.

Table 3
Comparison of TEM and XRD particle size for catalysts with different pore size.

Solids	Particle size (nm) (By TEM)	Particle size (nm) (By XRD)
Co-SBA-15-1	6.3	12.4
Co-SBA-15-8	14.4	18.7
Co-SBA-15-11	20.7	18.2

catalysts. However, significant differences in the intensity of the second band are evident, with the lower pore size catalyst showing a much more intense and sharp band compared to medium and large pore size catalysts. Table 4 shows the degree of reduction for all catalysts. As the pore size of the catalyst increases, the degree of reduction of the solid also increases, corroborating that the pore diameter of the support plays an important role influencing the particle size of the solid and its reducibility. The surface structure of the calcined catalysts was investigated by XPS analyses. Fig. 8 shows the spectrum obtained for catalyst Co-SBA-15-1 after calcination. Binding energies for Co species are presented in Table 5. For the Co, the spectra were fitted considering two-spin orbit doublets and four satellite peaks. We have adopted the criterion of fixing equal widths for the two main Co 2p3/2 lines of the two spin–orbit doublets. All samples show very similar Co $2p_{3/2}$ binding energy values. In all case, the most intense doublet and the shake up satellite can be assigned to Co^{2+}/Co^{3+} ions in the spinel phase of Co_3O_4

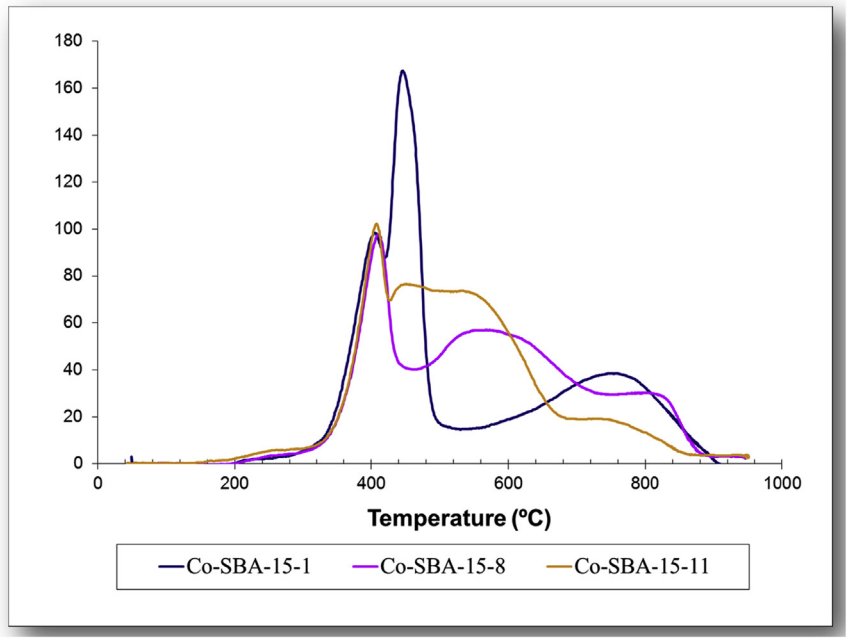

Fig. 6. TPR profiles of Co-SBA-15 catalysts.

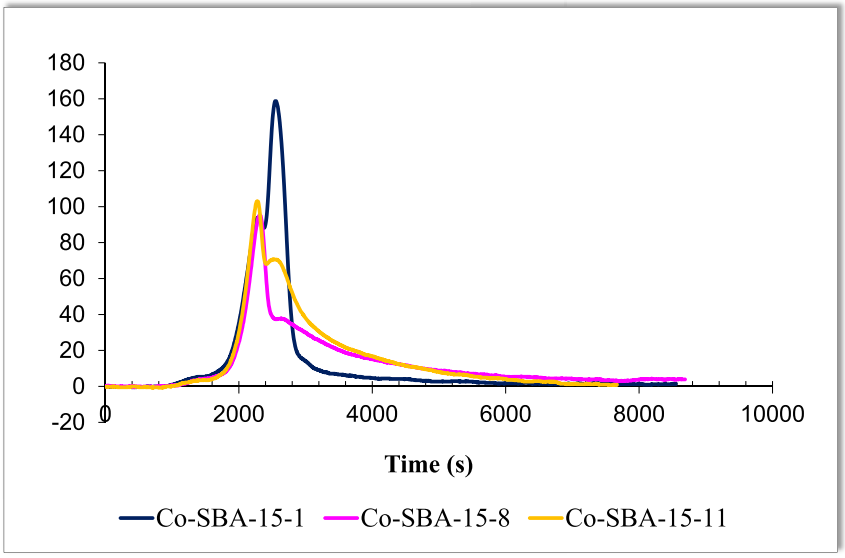

Fig. 7. TPR profiles at 400 °C for Co-SBA-15 catalysts.

Table 4
Reducibility of catalysts at T = 400° C.

	Co-SBA-15-1	Co-SBA-15-8	Co-SBA-15-11
Hydrogen consumption ($\mu molH_2\ g^{-1}cat$)	4553	5064	5681
Reducibility (%)	67	75	84

[26]. These results corroborate that the predominant phase in these oxide catalysts corresponds to Co_3O_4, in agreement with XRD results. The less intense doublet can be assigned to Co^{+2}.

3.3. Catalytic test Fischer–Tropsch synthesis

Fig. 9 shows the evolution of CO conversion with time on stream for the three studied catalysts. Initially, all catalysts showed high CO conversions with a marked tendency to deactivate. However, no significant differences were observed in terms of conversion values after reaching the steady state. This suggests that the FT reaction rate is not strongly affected by catalyst pore size. Initial deactivation of cobalt base catalysts for FT reaction has been largely debated and several explanations have arisen [27] Factors such as sintering of

Table 5
XPS cobalt binding energies.

Solids	Co2p $_{3/2}$ (eV) (More intense doublet)	Co2p $_{3/2}$ (eV) (Less intense doublet)
Co-SBA-15-1	779.30	780.6
Co-SBA-15-8	779.50	780.4
Co-SBA-15-11	779.40	780.4
Assignment	Co^{2+}/Co^{3+} ions in Co_3O_4	Co^{+2}

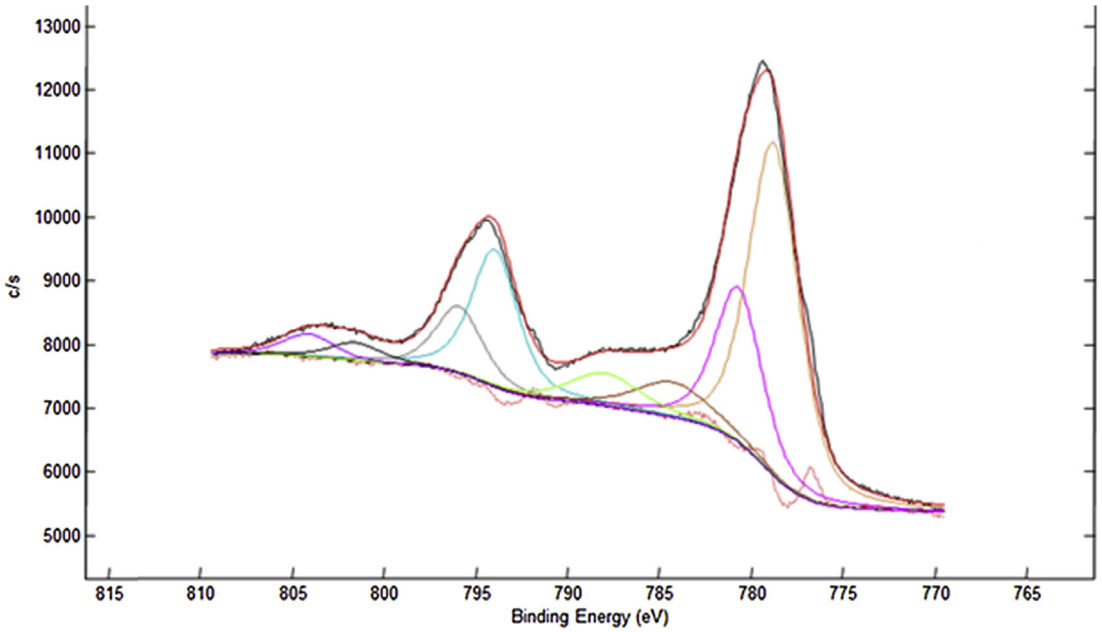

Fig. 8. XPS spectrum of the calcined Co-SBA-15-8 catalysts.

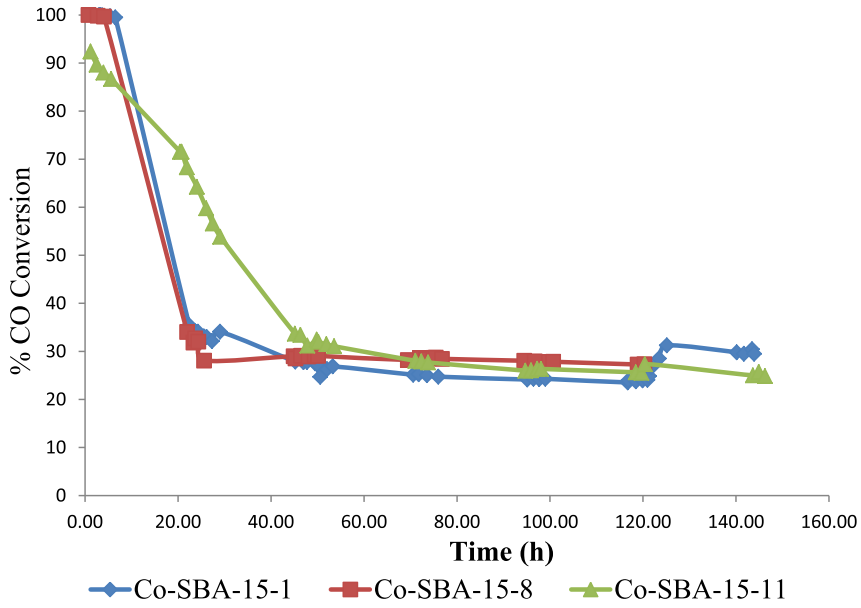

Fig. 9. Evolution of CO conversion with time on stream for Co-SBA-15catalysts.

metal particles, its re-oxidation under the hydrothermal environment generated during the reaction, diffusion effects due to condensation of reaction products and progressive filling of the pores, coke or graphite formations or, on ordered mesoporous materials, loss of the ordered structure of the support due to the conditions of temperature and pressure at which the solids are subjected during the reaction. Most of the research on cobalt catalyst deactivation in the last 15 years has been focused on the oxidation as a major mechanism for activity loss [28]. However, due to the complexity of the reaction, it is our believe that not a single effect can be invoked but several factors in association should cause the observed deactivation. The broad goal of the first stage of this project was no focused on study the deactivation mechanism for our catalysts. The FTS deactivation of cobalt supported catalyst for commercial application require testing catalysts for extended periods of time and under realistic FTS conditions. However, it is interesting to note that deactivation of Co-SBA-15-11 catalyst (large pore diameter) takes place slowly than the rest of the catalysts requiring a longer period of time (48 h) to reach steady state conditions (Fig. 9). It can be seen from Fig. 9 that the rate of Co-SBA-15-1 and Co-SBA-15-8 catalysts deactivation is much higher than that of Co-SBA-15-11 catalyst. Because catalyst Co-SBA-15-11 has the largest pore size, the filling of the pores with the liquid products should take longer. This seems to indicate that the primary cause of catalyst deactivation is related to reactant and products diffusion limitations.

Table 6 shows the results of conversion and product distribution obtained for the studied solids. The Co-SBA-15-1 catalyst with smaller pore size showed a lowest selectivity to methane. This result does not agree with the results reported by Anderson et al. [6] as they observed high methane selectivity when the pore size of the catalyst was small. They concluded that diffusion limitation of carbon monoxide in a small catalysts pore could increase H_2/CO ratio within the pore and thus increase the methane selectivity. However, our result can be explained in terms of the combining effect of high content and high dispersion of the metallic phase. The high metal loading allows for the small particles to be closer to each other, inducing CH_X monomers interaction and further chain growth. This phenomenon is also reflected in the C5+ selectivity trend. Even that the collected aqueous samples showed a small amount of oxygenates, mainly methanol, ethanol and 1-propanol, the selectivity to oxygenates was negligible for all studied catalysts.

Table 7 and Fig. 10 show the liquid hydrocarbons product distribution in the collected organic fraction. As previously reported [16], the distribution of liquid hydrocarbons varies significantly with catalyst pore size. Increasing catalyst pore size increases the selectivity toward heavier products. This seems to occur at the expense of the gasoline fraction, which decreases with increasing pore size. In fact, the observed behavior can be related to the ability of the liquid hydrocarbons chain (non-compressible) to grow inside a pore of limited space.

The observed trend seems contradictory to the results shown in Table 6 where selectivity towards C5+ decreased with increasing pore size: the amount of ***total*** liquid hydrocarbon is higher for catalyst Co-SBA-15-1 but the amount of ***heavy*** hydrocarbons is higher for catalysts Co-SBA-15-11.

A larger pore diameter could favor hydrocarbons growth within the pore and promotes formation of higher molecular weight products while a small pore diameter will limit chain growth favoring formation of lighter species. In the absence of the molecular sieve component, the liquid product comprises essentially waxy normal olefins and paraffin's, according to chain growth mechanism, which can be described by an Anderson- Schulz-Flory

Table 6
Conversion and standard product distribution obtained for studied catalysts.

Catalyst	XCO	%SCO_2	%SCH_4	%SC_2–C_4	%SC_{5+}	%Soxig
Co-SBA-15-1	28	3	25	14	58	0
Co-SBA-15-8	29	2	32	12	54	0
Co-SBA-15-11	28	6	32	13	49	0

Table 7
Liquid hydrocarbons Product Distribution.

	C_5–C_{10} Gasoline	C_{11}–C_{18} Diesel	C_{19+} Heavy hydrocarbons
Co-SBA-15-1	60	36	4
Co-SBA-15-8	49	41	10
Co-SBA-15-11	44	41	15

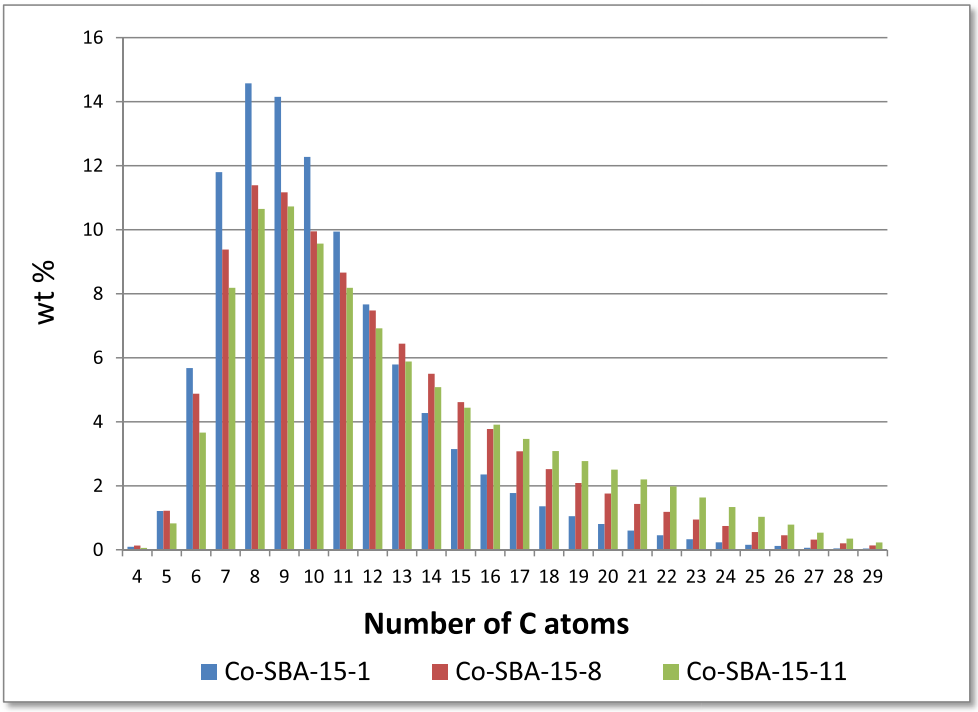

Fig. 10. Comparison of the liquid hydrocarbons product distribution for the studied catalysts.

equation.

From the hydrocarbon product distribution, the chain growth parameter alpha was calculated, which depends on the catalyst used and reaction conditions.

For a cobalt based catalyst, Dry et al. [29] reported typical $\alpha = 0.75–0.80$ values. From Table 8 it can clearly be seen how increasing the pore size of the catalyst increases the α parameter Co-SBA-15-8 and Co-SBA-15-11catalysts showed α parameter values within the range reported for Co-based catalysts. This result suggests that, for these catalysts, the synthesis of hydrocarbons via SFT is governed by an Anderson-Schulz-Flory (ASF) distribution. However, Co-SBA-15-1 catalyst with smaller pore size, showed a lower α value than the one reported in the literature, suggesting that the synthesis of hydrocarbons production in this case presents a deviation from the ASF mechanism. This deviation can be directly related with the shape selectivity effect exerted by the pores structure of the support on the liquid product distribution.

4. Conclusions

The broad goal of the first stage of this project was to synthesize and evaluate catalysts to produce diesel fraction components avoiding excess yields of both light hydrocarbons and heavy waxes.

Shape-selective catalysts had the potential to limit long-chain products and produce a non-Anderson- Schulz–Flory product distribution.

Pore diameter not only affects the size and reducibility of cobalt particles but significantly influences the liquid products distribution. By increasing catalysts pore size, a shift occurs in product distribution towards heavier hydrocarbon fractions, suggesting that the chain growth is highly influenced by the catalysts pore size. Small pores seem to limit polymeric chain growth favoring higher selectivity toward lower molecular weight products. This result leads us to conclude that the pore size of the catalyst induces a shape selectivity effect on the liquid hydrocarbons distribution obtained in the Fischer Tropsch reaction. A larger pore size also allows obtaining bigger cobalt oxide particles which can be reduced more easily ensuring higher surface concentration of metallic cobalt, responsible for catalytic activity in the FTS.

Table 8
Chain growth parameter (α).

Catalysts	Parameter α
Co-SBA-15-1	0.72
Co-SBA-15-8	0.78
Co-SBA-15-11	0.83

Acknowledgments

The authors are grateful for financial support from the Council of Scientific and Humanistic Development of Venezuelan Central University (UCV-CDCH) through project CDCH PG-03-7903-2009.

References

[1] M.E. Dry, J. Chem. Technol. Biotechnol. 77 (2001) 43–50.
[2] I. Puskas, R.S. Hurlbut, Catal. Today 84 (2003) 99–109.
[3] J. van de Loosdrecht, B. Balzhinimaev, J.-A. Dalmon, J.W. Niemantsverdriet, S.V. Tsybulya, A.M. Saib, P.J. van Berge, J.L. Visage, Catal. Today 123 (2007) 293–302.
[4] A.M. Saib, D.J. Moodley, I.M. Ciobica, M.M. Hauman, B.H. Sigwebela, C.J. Weststrate, J.W. Niemantsverdriet, J. van de Loosdrecht, Catal. Today 154 (2010) 271–282.
[5] G.P. Van Der Laan, A.A.C.M. Beenackers, Catal. Rev. Sci. Eng 41 (1999) 255–318.
[6] A.C. Vosloo, Fuel Process. Technol. 71 (2001) 149–155.
[7] E. Iglesia, App. Catal. A General 161 (1997) 59–78.
[8] A.K. Dalai, B.H. Davis, App. Catal. A General 348 (2008) 1–15.
[9] K. Okabe, X.H. Li, M.D. Wei, H. Arakawa, Catal. Today 89 (2004) 431–438.
[10] R.B. Anderson, W.K. Hall, A. Krieg, B. Seligman, J. Am. Chem. Soc. 71 (1949) 183–188.
[11] J.A. Lapszewicz, H.J. Loeh, J.R. Chipperfield, J. Chem. Soc. Chem. Commun. (1993) 913–914.
[12] B. Ernst, S. Libs, P. Chaumette, A. Kiennemann, Appl. Catal. A: Gen. 186 (1999)

145–168.
[13] Y. Khodakov, A.G. Constant, R. Bechara, V.L. Zholobenko, J. Catal. 206 (2002) 230–241.
[14] E. Iglesia, S.L. Soled, J.E. Baumgartner, S.C. Reyes, J. Catal. 153 (1995) 108–122.
[15] Feller, M. Claeys, E. van Steen, J. Catal. 185 (1999) 120–130.
[16] A.M. Saib, M. Claeys, E. van Steen, Catal. Today 71 (2002) 395–402.
[17] H. Xiong, Y. Zhang, K. Liew, J. Li, J. Molec. Catal. A: Chem. 295 (2008) 68–76.
[18] E. Lira, C.M. Lopez, F. Oropeza, M. Bartolini, J. Alvarez, M. Goldwasser, F. Lopez Linares, J.F. Lamonier, M.J. Perez Zurita, J. Molec. Catal. 281 (2008) 146–153.
[19] Y. Wang, M. Noguchi, Y. Takahashi, Y. Ohtsuka, Catal. Today 68 (2001) 3–9.
[20] L. Katiyar, P. Ji, N.G. Smirniotis, Pinto, J. Chromatogr. A 1069 (2005) 119–126.
[21] T. Phuong, B. Nguyen, J.W. Lee, W.G. Shim, H. Moon, Microporous Mesoporous Mater. 110 (2008) 560–569.
[22] M.C.J. Bradford, M.A. Vannice, Appl. Catal. A: Gen. 142 (1996) 73–96.
[23] H.P. Klug, L.E. Alexander, X-ray Diffraction Procedures for Polycrystalline and Amorphous Materials, Wiley, London, 1962, p. 491.
[24] D. Song, J. Li, J. Mol. Catal. A: Chem. 247 (2006) 206–212.
[25] Y. Khodakov, R. Bechara, A. Griboval-Constant, App. Catal. 254 (2003) 273–288.
[26] E. Steen Van, M. Claeys, A.M. Saib, Catal. Today 71 (2002) 395–402.
[27] K. Khodakov, A. Griboval-Constant, J. Catal. 206 (2002) 230–241.
[28] Martínez, C. López, F. Márquez e, I. Díaz, J. Catal. 220 (2003) 486–499.
[29] M.E. Dry, J. Mol. Catal. 17 (1982) 133–144.